cost and the preprocessing of geometric and radiometric corrections of satellite imagery, exemplified by the Landsat program. Given such progressive data policies and image processing capabilities, it is now possible to use advanced computing systems, such as the Google cloud, to efficiently process and characterize global-scale time-series data sets in quantifying land change. There are several satellite systems in place or planned for collecting data with similar capabilities to Landsat. Similar free and open data policies would enable greater use of these data for public good and foster greater transparency of the development, implementation, and reactions to policy initiatives that affect the world's forests.

The information content of the presented data sets, which are publicly available, provides a transparent, sound, and consistent basis on which to quantify critical environmental issues, including (i) the proximate causes of the mapped forest disturbances (*15*); (ii) the carbon stocks and associated emissions of disturbed forest areas (*16*–*18*); (iii) the rates of growth and associated carbon stock gains for both managed and unmanaged forests (*19*); (iv) the status of remaining intact natural forests of the world and threats to biodiversity (*20*, *21*); (v) the effectiveness of existing protected-area networks (*22*); (vi) the economic drivers of natural forest conversion to more intensive land uses (*23*); (vii) the relationships between forest dynamics and social welfare, health, and other relevant human dimensions data; (viii) forest dynamics associated with governance and policy actions—and many other regional-to-global–scale applications.

References and Notes

1. J. A. Foley *et al.*, *Science* **309**, 570–574 (2005).
2. M. C. Hansen, S. V. Stehman, P. V. Potapov, *Proc. Natl. Acad. Sci. U.S.A.* **107**, 8650–8655 (2010).
3. Food and Agricultural Organization of the United Nations, *Global Forest Land-Use Change 1990-2005, FAO Forestry Paper No. 169* (Food and Agricultural Organization of the United Nations, Rome, 2012).
4. M. Hansen, R. DeFries, *Ecosystems* **7**, 695–716 (2004).
5. Instituto Nacional de Pesquisas Especias, *Monitoring of the Brazilian Amazonian Forest by Satellite, 2000-2012* (Instituto Nacional de Pesquisas Especias, San Jose dos Campos, Brazil, 2013).
6. G. Sparovek, G. Berndes, A. G. O. P. Barretto, I. L. F. Klug, *Environ. Sci. Policy* **16**, 65–72 (2012).
7. D. P. Edwards, W. F. Laurance, *Nature* **477**, 33 (2011).
8. M. Drummond, T. Loveland, *Bioscience* **60**, 286–298 (2010).
9. W. A. Kurz *et al.*, *Nature* **452**, 987–990 (2008).
10. B. Gardiner *et al.*, *Destructive Storms in European Forests: Past and Forthcoming Impacts* (European Forest Institute, Freiburg, Germany, 2010).
11. P. Potapov, M. Hansen, S. Stehman, T. Loveland, K. Pittman, *Remote Sens. Environ.* **112**, 3708–3719 (2008).
12. A. Prishchepov, D. Muller, M. Dubinin, M. Baumann, V. Radeloff, *Land Use Policy* **30**, 873–884 (2013).
13. United Nations Framework Convention on Climate Change, *Reducing Emissions from Deforestation in Developing Countries: Approaches to Stimulate Action – Draft Conclusions Proposed by the President* (United Nations Framework Convention on Climate Change Secretariat, Bonn, Germany, 2005).
14. R. Houghton *et al.*, *Carbon Manage.* **1**, 253–259.
15. H. Geist, E. Lambin, *Bioscience* **52**, 143–150 (2002).
16. S. S. Saatchi *et al.*, *Proc. Natl. Acad. Sci. U.S.A.* **108**, 9899–9904 (2011).
17. A. Baccini *et al.*, *Nature Clim. Change* **2**, 182–185 (2012).
18. N. L. Harris *et al.*, *Science* **336**, 1573–1576 (2012).
19. R. Waterworth, G. Richards, C. Brack, D. Evans, *For. Ecol. Manage.* **238**, 231–243 (2007).
20. P. Potapov *et al.*, *Ecol. Soc.* **13**, 51 (2008).
21. T. M. Brooks *et al.*, *Science* **313**, 58–61 (2006).
22. A. S. Rodrigues *et al.*, *Nature* **428**, 640–643 (2004).
23. T. Rudel, *Rural Sociol.* **63**, 533–552 (1998).

Acknowledgments: Support for Landsat data analysis and characterization was provided by the Gordon and Betty Moore Foundation, the United States Geological Survey, and Google, Inc. GLAS data analysis was supported by the David and Lucile Packard Foundation. Development of all methods was supported by NASA through its Land Cover and Land Use Change, Terrestrial Ecology, Applied Sciences, and MEaSUREs programs (grants NNH05ZDA001N, NNH07ZDA001N, NNX12AB43G, NNX12AC78G, NNX08AP33A, and NNG06GD95G) and by the U.S. Agency for International Development through its CARPE program. Any use of trade, firm, or product names is for descriptive purposes only and does not imply endorsement by the U.S. government. Results are depicted and viewable online at full resolution: http://earthenginepartners.appspot.com/science-2013-global-forest.

Supplementary Materials

www.sciencemag.org/content/342/6160/850/suppl/DC1
Materials and Methods
Supplementary Text
Figs. S1 to S8
Tables S1 to S5
References (*24*–*40*)

14 August 2013; accepted 15 October 2013
10.1126/science.1244693

Changes in Cytoplasmic Volume Are Sufficient to Drive Spindle Scaling

James Hazel,[1] Kaspars Krutkramelis,[2] Paul Mooney,[1] Miroslav Tomschik,[1] Ken Gerow,[3] John Oakey,[2] J. C. Gatlin[1]*

The mitotic spindle must function in cell types that vary greatly in size, and its dimensions scale with the rapid, reductive cell divisions that accompany early stages of development. The mechanism responsible for this scaling is unclear, because uncoupling cell size from a developmental or cellular context has proven experimentally challenging. We combined microfluidic technology with *Xenopus* egg extracts to characterize spindle assembly within discrete, geometrically defined volumes of cytoplasm. Reductions in cytoplasmic volume, rather than developmental cues or changes in cell shape, were sufficient to recapitulate spindle scaling observed in *Xenopus* embryos. Thus, mechanisms extrinsic to the spindle, specifically a limiting pool of cytoplasmic component(s), play a major role in determining spindle size.

Organelles and other intracellular structures must scale with cell size in order to function properly. Maintenance of these dimensional relationships is challenged by the rapid and reductive cell divisions that characterize early embryogenesis in many organisms. The cellular machine that drives these divisions, the mitotic spindle, functions to segregate chromosomes in cells that vary greatly in size while also adapting to rapid changes in cell size. The issue of scale is epitomized during *Xenopus* embryogenesis, where a rapid series of divisions reduces cell size 100-fold: from the 1.2-mm-diameter fertilized egg to ~12-μm-diameter cells in the adult frog (*1*). In large blastomeres, spindle length reaches an upper limit that is uncoupled from changes in cell size. However, as cell size decreases, a strong correlation emerges between spindle length and cell size (*2*). Although this scaling relationship has been characterized in vivo for several different organisms, little is known about the direct regulation of spindle size by cell size or the underlying mechanism(s) (*2*–*4*). Spindle size may be directly dictated by the physical dimensions of a cell, perhaps through microtubule-mediated interaction with the cell cortex [i.e., boundary sensing (*5*–*7*)]. Alternatively, cell size could constrain spindle size by providing a fixed and finite cytoplasmic volume and, therefore, a limiting pool of resources such as cytoplasmic spindle assembly or length-determining components [i.e., component limitation (*8*, *9*)]. Last, mechanisms intrinsic to the spindle could be actively tuned in response to systematic changes in cytoplasmic composition occurring during development [i.e., developmental cues (*10*, *11*)].

To elucidate the responsible scaling mechanism(s), we developed a microfluidic-based platform to confine spindle assembly in geometrically defined volumes of *Xenopus* egg extract (*12*). Interphase extract containing *Xenopus* sperm nuclei was induced to enter mitosis and immediately pumped into a microfluidic droplet-generating device before nuclear envelope breakdown and the onset of spindle assembly. At the same time, a fluorinated oil/surfactant mixture was pumped into the device through a second inlet. These two discrete, immiscible phases merged at a T-shaped junction within the device to produce stable emulsions of extract droplets in a continuous oil phase (Fig. 1, A and C). Changing the T-junction channel dimensions and relative flow rates of the two phases

[1]Department of Molecular Biology, University of Wyoming, Laramie, WY 82071, USA. [2]Department of Chemical and Petroleum Engineering, University of Wyoming, Laramie, WY 82071, USA. [3]Department of Statistics, University of Wyoming, Laramie, WY 82071, USA.

*Corresponding author. E-mail: jgatlin@uwyo.edu

Downloaded from www.sciencemag.org on April 4, 2015

enabled us to tune droplet volume. Droplet shape could be controlled independently by changing the geometry and dimensions of the device's collection region. In this way, we were able to produce three distinct geometries: spheres, flattened discs, and axially elongated "slugs" (Fig. 1, B and C). After encapsulation, nuclei size and shape resembled those of their unencapsulated counterparts (Fig. 1C), suggesting that the process of droplet generation did not appreciably perturb nuclear morphology.

To examine the relationship between steady-state spindle length and cytoplasmic volume, we encapsulated interphase nuclei within spherical droplets ranging in diameter from 20 to 120 μm. Bipolar spindle assembly was observed in droplets of greater than ~30 μm diameter, permitting measurements of spindle length by using fluorescence microscopy (Fig. 2, A and B). Spindles exhibited isometric scaling, so we used the single metric of spindle length to serve as a reasonable proxy for spindle size (Fig. 2A). This also allowed direct comparisons with previously published scaling data in which length was the only reported spindle dimension. These measurements defined two distinct regimes that described the relationship between spindle length and droplet

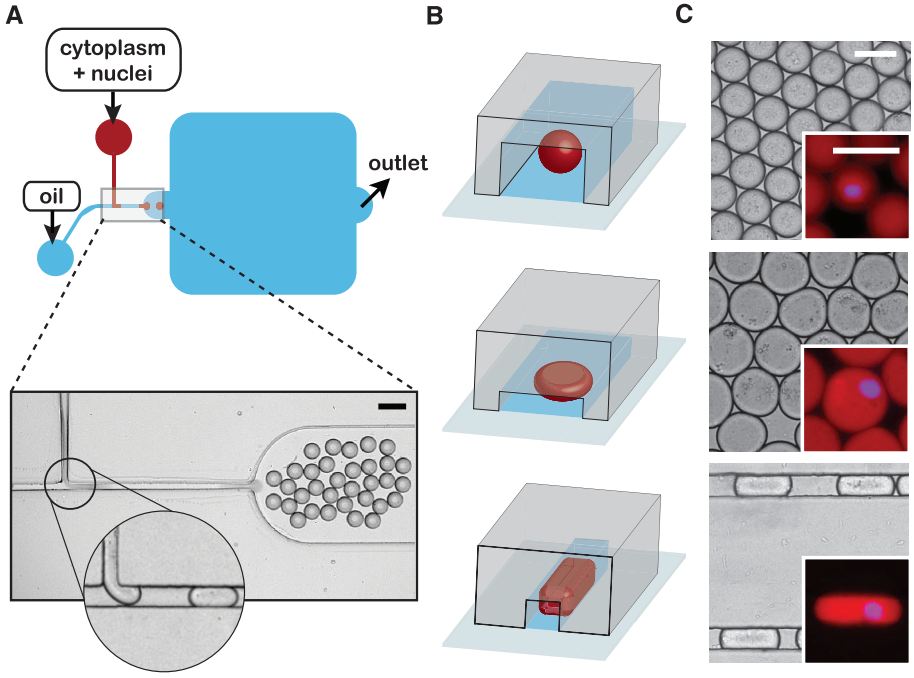

Fig. 1. Microfluidic encapsulation of nuclei in cytoplasmic volumes of defined size and shape. (**A**) (Top) Simplified schematic of a polydimethylsiloxane microfluidic device featuring a classic T-junction droplet generator and collection reservoir (blue rounded square). An extract phase containing nuclei (red) is continuous until sheared off into droplets by the oil/surfactant phase (blue). (Bottom) A representative image of droplet generation at a standard T-junction. (Inset) A formed droplet moving toward the collection reservoir and another about to be sheared from the extract phase (movie S1). Scale bar indicates 100 μm. (**B**) Alternative droplet shapes result from changing the collection reservoir geometry: spheres (top), flattened disks (middle), and elongated slug-shaped droplets (bottom). (**C**) Representative micrographs of spheres, discs, and slugs contained within reservoirs or channels. Scale bar, 50 μm. (Insets) Magnified images of droplets encapsulating "cycled" interphase sperm nuclei. Nuclear DNA was stained with 4′,6-diamidino-2-phenylindole (DAPI) to access nuclear morphology (blue), and soluble tubulin (pseudo-colored red, labeled with Atto-488) was used to visualize droplet boundaries. All droplets are roughly isovolumetric. Inset scale bar, 50 μm.

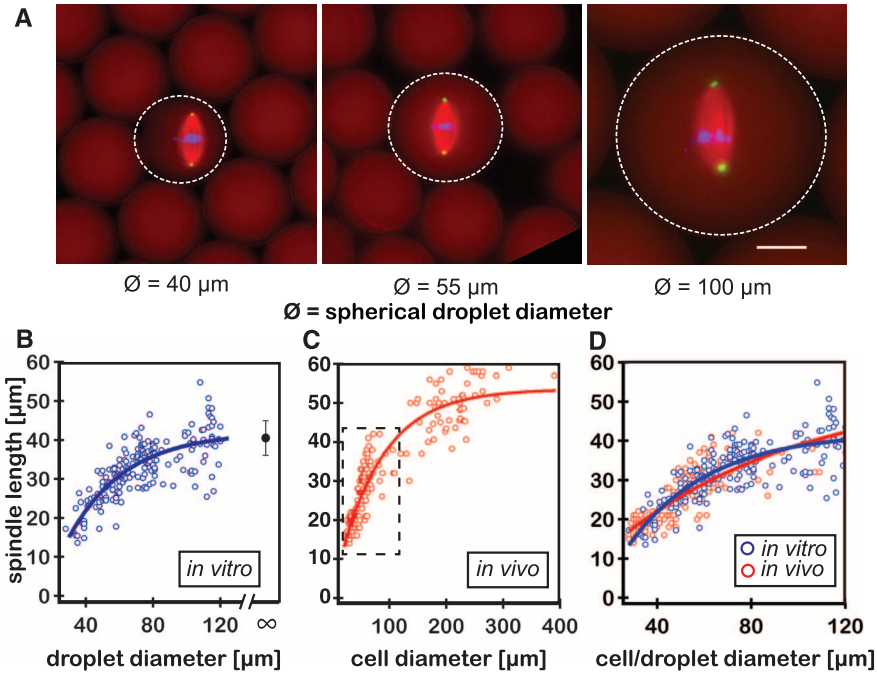

Fig. 2. Developmental spindle scaling can be recapitulated in vitro in the absence of developmental cues or a functional cell cortex. (**A**) Representative fluorescent images of spindles assembled in spherical extract droplets of various sizes. Spindles were labeled by adding fluorophores to the extract before droplet formation; tubulin was added to visualize microtubules (pseudo-colored red, labeled with Atto-488); DAPI, to visualize DNA (blue); and antibodies against nuclear mitotic apparatus protein (NuMA), to visualize spindle poles (pseudo-colored green, directly labeled with Atto-568). Dashed circles indicate droplet boundaries as visualized by the extent of soluble labeled tubulin. Scale bar, 25 μm. (**B**) Spindle length plotted as a function of encapsulating droplet diameter (blue open circles, n = 96 spindles). The single black circle indicates the average spindle length in unencapsulated extract (mean ± SD; n = 81 spindles). (**C**) Spindle length at metaphase plotted as a function of cell size during early (stages 8 to 9) *Xenopus* embryo development [red open circles; adapted from (*2*)]. (**D**) Comparison of spindle scaling in vitro and in vivo (blue and red open circles, respectively, with corresponding fits). Each data set was fit by using a three-parameter equation that assumes asymptotic growth [solid lines in (B) to (D) and figs. S1 and S2].

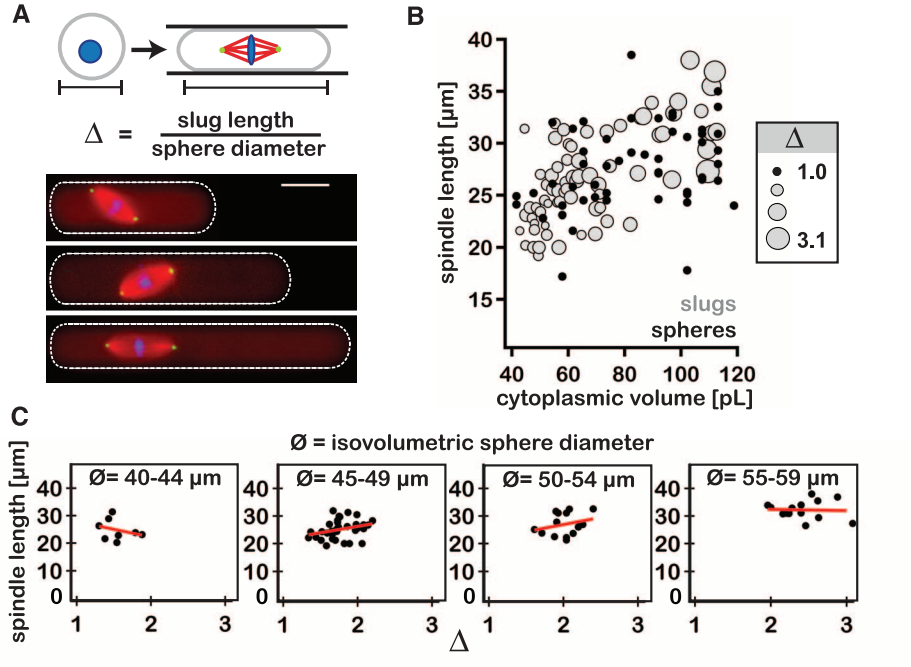

Fig. 3. Reductions in cytoplasmic volume account for the spindle scaling observed in vitro. (**A**) (Top) Cartoon depicting the transformation of a spherical droplet into an isovolumetric slug and the calculation of extent of elongation (Δ). (Bottom) Fluorescent images of representative spindles assembled in slugs of increasing Δ. Fluorophores were added to the extract as described in Fig. 2. (**B**) Spindle length plotted as a function of droplet cytoplasmic volume. For shaded markers (gray circles, n = 71 spindles), marker size is proportional to the ratio of slug long-axis length over the diameter of an isovolumetric sphere (i.e., extent of elongation, denoted as Δ). Solid markers (black circles) represent data derived from spherical droplets (i.e., Δ = 1, n = 96 spindles). (**C**) Spindle length as a function of extent of elongation under near-isovolumetric conditions (i.e., binned by isovolumetric sphere diameter, Ø). Linear trend lines (red) exhibit variable slopes, indicating a lack of a constant relationship between the two measurements.

diameter: In droplets with diameters larger than ~80 μm, spindle length was relatively constant, reaching an upper limit similar to the average spindle length found in unencapsulated extract (~40.5 ± 4.4 μm; mean ± SD), whereas in smaller droplets spindle length scaled almost linearly with droplet diameter (Fig. 2B).

These results share notable similarity with spindle scaling observed during *Xenopus* development, particularly in the linear scaling regime (*2*) (Fig. 2, C and D). Within their respective scaling regimes, asymptotic growth fits to the in vivo and in vitro data sets were statistically indistinguishable (solid lines in Fig. 2, B to D; figs. S1 and S2), suggesting that our in vitro system recapitulated the scaling observed in vivo. Scaling was observed in droplets ranging in diameter from ~30 to 80 μm, corresponding to cell sizes typical of stages 8 and 9 of *Xenopus* development (Fig. 2D), a temporal window that encompasses the mid-blastula transition and the onset of zygotic transcription (*13*, *14*). Because *Xenopus* egg extracts are effectively static in a developmental context, changes in cytoplasmic composition that might affect scaling in the intact embryo do not occur in our system [e.g., (*15*)]. Thus, developmental cues can be eliminated as a potential model for the spindle scaling observed in these droplets, leaving the two remaining hypothetical mechanisms, component limitation and/or boundary sensing.

A boundary-sensing mechanism predicts that changing the physical dimensions of the encapsulating droplet, while holding droplet volume constant, should affect spindle length. To test this model, we compared the lengths of spindles assembled in spheres with those assembled in longer, isovolumetric slugs. The use of slugs as opposed to flattened spheres allowed spindle assembly to be restricted in two of three dimensions over a broader aspect ratio range (Fig. 3A). To ensure that encapsulated spindle lengths could vary in response to changes in droplet shape, we generated slugs by geometrically confining spheres ranging in diameter from 40 to 60 μm

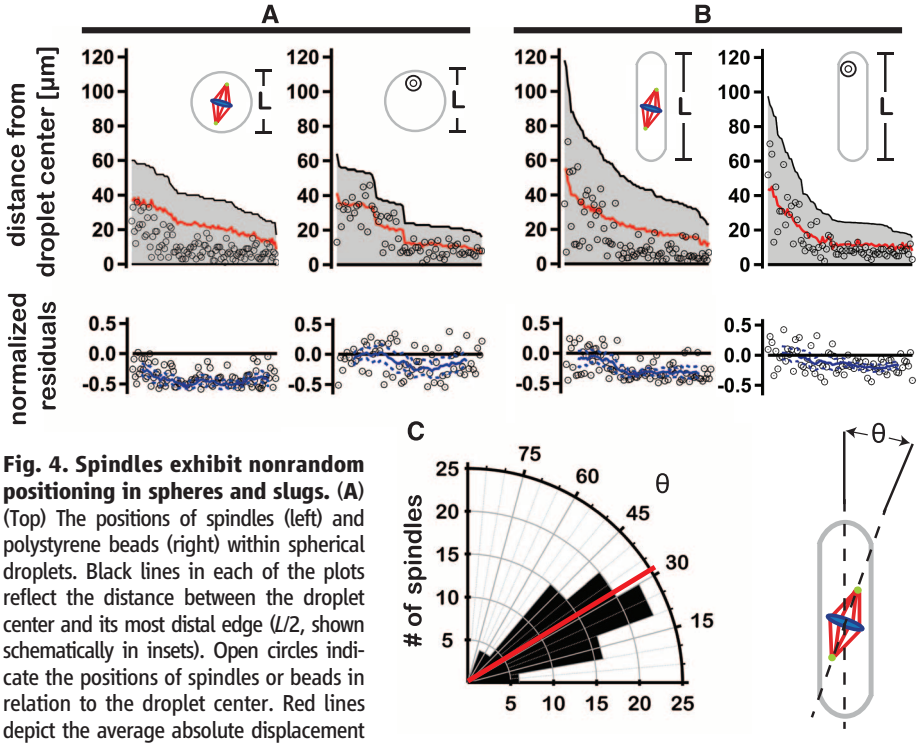

Fig. 4. Spindles exhibit nonrandom positioning in spheres and slugs. (**A**) (Top) The positions of spindles (left) and polystyrene beads (right) within spherical droplets. Black lines in each of the plots reflect the distance between the droplet center and its most distal edge (*L*/2, shown schematically in insets). Open circles indicate the positions of spindles or beads in relation to the droplet center. Red lines depict the average absolute displacement of spindles/beads expected for uniform random positioning (see supplementary materials). (Bottom) Corresponding residual plots show the normalized difference between the center-to-center position of the spindle or bead and the theoretical random position. Solid blue lines represent the moving average of residual values (with upper and lower 95% confidence intervals indicated by dashed blue lines). (**B**) As in (A), spindle and bead positions in axially elongated slugs. (**C**) Spindle orientation in slugs. (Left) Polar histogram plot showing the angle θ between the interpolar spindle axis and the long axis of the confining slug (red line indicates the average orientation angle; n = 89 spindles). (Right) Cartoon depicting the determination of angle θ.

(the approximate midpoint of the scaling regime; movie S2). Differences in spindle lengths for these two extract droplet geometries were statistically indistinguishable (Student's t test, $P = 0.2$ for all slug and sphere data between 40 and 60 μm). Furthermore, spindle length remained relatively constant despite threefold increases in slug length over a narrow range of cytoplasmic volumes (Fig. 3, B and C, and fig. S3). Collectively, these results oppose the predictions of a boundary-sensing model for spindle length regulation and suggest that cytoplasmic shape is not likely a major determinant of spindle length.

Through a variety of different mechanisms, spindles in vivo demonstrate a remarkable ability to correctly position themselves near the cell center before the onset of anaphase and cytokinesis. (*16*–*20*). Each implicitly requires the spindle be able to "sense" its position relative to cellular boundaries. In the absence of boundary sensing, spindle position within a cell (or a confining extract volume) is expected to be random. To test this prediction, we plotted spindle position relative to the volumetric centers of confining spheres and slugs (Fig. 4, A and B). In both geometries, spindles tended to localize toward the droplet center to a greater extent than expected for uniform random positioning (Fig. 4, A and B, and movie S3). This trend was more pronounced in smaller droplets (Fig. 4, A and B, residual plots). In contrast, the positions of encapsulated polystyrene beads aligned more closely with average random positions (Fig. 4, A and B, residual plots; figs. S1 and S2; and movie S4). This suggested that the weak convective flows observed in some slugs were likely not responsible for spindle centering (e.g., movie S5). The distribution of spindle orientations relative to the slug long axis was found to be 31° ± 16° (Fig. 4C), indicating that, like in cells, a spindle is more likely to align parallel to the long axis of its enclosure (*21*), even in the absence of a cortical membrane and associated pulling forces. Indeed, peripheral spindle microtubules extend well beyond the spindle proper, effectively increasing its size (*22*). Perhaps these peripheral microtubules exert pushing forces against droplet boundaries that result in centering (*23*). Alternatively, spindle proximity to a droplet boundary might influence the distribution of forces generated by microtubule-associated motors pulling against the bulk cytoplasm (*19*, *24*). Thus, a boundary-sensing mechanism might indeed work to affect spindle position but contributes little, if at all, to determining spindle length.

Collectively, our data indicate that changes in cytoplasmic volume are sufficient to account for spindle scaling as it occurs in vivo (*2*). By eliminating alternative hypothetical models, the data support a scaling mechanism in which a limiting pool of cytoplasmic component(s) regulates spindle length (*8*, *11*). In large droplets or cells, like in unbounded extract, spindle length appears to be constrained by mechanisms intrinsic to the spindle (*2*, *25*). Once cytoplasmic volume is reduced to a critical threshold, components become limited, which produces smaller spindles. This process serves as a passive yet robust way for cells to control the size of their spindles and possibly other internal structures.

References and Notes

1. M. Montorzi, M. H. Burgos, K. H. Falchuk, *Mol. Reprod. Dev.* **55**, 75–82 (2000).
2. M. Wühr *et al.*, *Curr. Biol.* **18**, 1256–1261 (2008).
3. A. Courtois, M. Schuh, J. Ellenberg, T. Hiiragi, *J. Cell Biol.* **198**, 357–370 (2012).
4. Y. Hara, A. Kimura, *Curr. Biol.* **19**, 1549–1554 (2009).
5. S. L. Bird, R. Heald, K. Weis, *Mol. Biol. Cell* **24**, 2506–2514 (2013).
6. T. Kiyomitsu, I. M. Cheeseman, *Nat. Cell Biol.* **14**, 311–317 (2012).
7. D. J. Sharp *et al.*, *Mol. Biol. Cell* **11**, 241–253 (2000).
8. M. Decker *et al.*, *Curr. Biol.* **21**, 1259–1267 (2011).
9. W. B. Ludington, L. Z. Shi, Q. Zhu, M. W. Berns, W. F. Marshall, *Curr. Biol.* **22**, 2173–2179 (2012).
10. Y. H. Chan, W. F. Marshall, *Organogenesis* **6**, 88–96 (2010).
11. N. W. Goehring, A. A. Hyman, *Curr. Biol.* **22**, R330–R339 (2012).
12. A. Desai, A. W. Murray, T. Mitchison, C. E. Walczak, in *Mitosis and Meiosis*, C. L. Rieder, vol. 61 of *Methods in Cell Biology* (Academic Press, New York, 1999), pp. 385–412.
13. J. Newport, M. Kirschner, *Cell* **30**, 675–686 (1982).
14. P. D. Nieuwkoop, J. Faber, Eds., *Normal Table of* Xenopus laevis *[Daudin] - A Systematical and Chronological Survey of the Development from the Fertilized Egg Till the End of Metamorphosis* (North-Holland, Amsterdam, ed. 2, 1967).
15. J. D. Wilbur, R. Heald, *Elife* **2**, e00290 (2013).
16. P. Gönczy, S. Grill, E. H. Stelzer, M. Kirkham, A. A. Hyman, in *The Cell Cyle and Development*, G. R. Bock, G. Cardew, J. A. Goode, Eds. (Novartis Foundation Symposium no. 237, Wiley, Chichester, UK, 2008), pp. 164–181.
17. L. Lee *et al.*, *Science* **287**, 2260–2262 (2000).
18. N. Minc, D. Burgess, F. Chang, *Cell* **144**, 414–426 (2011).
19. T. Mitchison *et al.*, *Cytoskeleton* **69**, 738–750 (2012).
20. I. M. Tolić-Nørrelykke, L. Sacconi, G. Thon, F. S. Pavone, *Curr. Biol.* **14**, 1181–1186 (2004).
21. M. Wühr, E. S. Tan, S. K. Parker, H. W. Detrich 3rd, T. J. Mitchison, *Curr. Biol.* **20**, 2040–2045 (2010).
22. J. C. Gatlin *et al.*, *Curr. Biol.* **19**, 287–296 (2009).
23. T. E. Holy, M. Dogterom, B. Yurke, S. Leibler, *Proc. Natl. Acad. Sci. U.S.A.* **94**, 6228–6231 (1997).
24. M. Wühr, S. Dumont, A. C. Groen, D. J. Needleman, T. J. Mitchison, *Cell Cycle* **8**, 1115–1121 (2009).
25. S. Dumont, T. J. Mitchison, *Curr. Biol.* **19**, R749–R761 (2009).

Acknowledgments: We thank T. Salmon and T. Mitchison for their insightful reviews of the manuscript; M. Wuhr for comments on the work and for providing access to raw data originally presented in (*2*); L. Edens, C. Geisler, D. Fay, and D. Levy in the Molecular Biology Department at the University of Wyoming for their critical review of the manuscript and helpful suggestions; and A. Groen for providing labeled anti-NuMA used in these studies. This work was supported by NIH grants R01 GM102428 (to J.C.G.) and R15 GM101636 (to J.O.) and by the NIH-funded Wyoming IDeA Networks of Biomedical Research Excellence program (P20RR016474 and P20GM103432).

Supplementary Materials

www.sciencemag.org/content/342/6160/853/suppl/DC1
Materials and Methods
Supplementary Text
Figs. S1 to S3
References (*26*–*31*)
Movies S1 to S5

12 July 2013; accepted 15 October 2013
10.1126/science.1243110

Cytoplasmic Volume Modulates Spindle Size During Embryogenesis

Matthew C. Good,[1,2,3] Michael D. Vahey,[2] Arunan Skandarajah,[2] Daniel A. Fletcher,[2,4]* Rebecca Heald[1]*

Rapid and reductive cell divisions during embryogenesis require that intracellular structures adapt to a wide range of cell sizes. The mitotic spindle presents a central example of this flexibility, scaling with the dimensions of the cell to mediate accurate chromosome segregation. To determine whether spindle size regulation is achieved through a developmental program or is intrinsically specified by cell size or shape, we developed a system to encapsulate cytoplasm from *Xenopus* eggs and embryos inside cell-like compartments of defined sizes. Spindle size was observed to shrink with decreasing compartment size, similar to what occurs during early embryogenesis, and this scaling trend depended on compartment volume rather than shape. Thus, the amount of cytoplasmic material provides a mechanism for regulating the size of intracellular structures.

Although mechanisms that set eukaryotic cell size by coordinating growth and division rates have been uncovered (*1*–*3*), much less is known about how the size and the shape of a cell affect its physiology. Recent work has suggested mechanisms by which cell boundaries or size can control biochemical reactions (*2*), constrain cytoskeletal assembly (*4*–*6*), and dictate the positioning of internal structures (*7*, *8*). The size-scaling problem is most acute during early embryo development, when cell size changes rapidly. For example, over the first 10 hours of amphibian embryogenesis, cell diameter may decrease 100-fold, from a 1.2-mm egg to 12-μm-diameter blastomeres, because of cell division in

[1]Department of Molecular and Cellular Biology, University of California–Berkeley, Berkeley, CA 94720, USA. [2]Department of Bioengineering and Biophysics Group, University of California–Berkeley, Berkeley, CA 94720, USA. [3]Miller Institute for Basic Research in Science, University of California–Berkeley, Berkeley, CA 94720, USA. [4]Physical Biosciences Division, Lawrence Berkeley National Laboratory, Berkeley, CA 94720, USA.

*Corresponding author. E-mail: bheald@berkeley.edu (R.H.), fletch@berkeley.edu (D.A.F.)

EXTENDED PDF FORMAT
SPONSORED BY


http://www.rndsystems.com/rnd_page_objectname_sample_size_antibodies.aspx?utm_source=Science.com&utm_medium=PDF&utm_campaign=Sample%20Size%20Antibodies

Changes in Cytoplasmic Volume Are Sufficient to Drive Spindle Scaling

James Hazel *et al.*

Science **342**, 853 (2013);
DOI: 10.1126/science.1243110

This copy is for your personal, non-commercial use only.

If you wish to distribute this article to others, you can order high-quality copies for your colleagues, clients, or customers by clicking here.

Permission to republish or repurpose articles or portions of articles can be obtained by following the guidelines here.

The following resources related to this article are available online at www.sciencemag.org (this information is current as of April 4, 2015):

Updated information and services, including high-resolution figures, can be found in the online version of this article at:
http://www.sciencemag.org/content/342/6160/853.full.html

Supporting Online Material can be found at:
http://www.sciencemag.org/content/suppl/2013/11/13/342.6160.853.DC1.html

A list of selected additional articles on the Science Web sites **related to this article** can be found at:
http://www.sciencemag.org/content/342/6160/853.full.html#related

This article **cites 27 articles**, 6 of which can be accessed free:
http://www.sciencemag.org/content/342/6160/853.full.html#ref-list-1

This article has been **cited by** 10 articles hosted by HighWire Press; see:
http://www.sciencemag.org/content/342/6160/853.full.html#related-urls

This article appears in the following **subject collections:**
Cell Biology
http://www.sciencemag.org/cgi/collection/cell_biol

Downloaded from www.sciencemag.org on April 4, 2015

Science (print ISSN 0036-8075; online ISSN 1095-9203) is published weekly, except the last week in December, by the American Association for the Advancement of Science, 1200 New York Avenue NW, Washington, DC 20005. Copyright 2013 by the American Association for the Advancement of Science; all rights reserved. The title *Science* is a registered trademark of AAAS.